Multiscale Directional Transforms based on Cosine-Sine Modulated Filter Banks for Sparse Directional Image Representation

Yusuke Nomura*, Ryutaro Ogawa*, Seisuke Kyochi*, and Taizo Suzuki†
* The University of Kitakyushu, Fukuoka, Japan
E-mail: s-kyochi@kitakyu-u.ac.jp
† University of Tsukuba, Ibaraki, Japan
E-mail: taizo@cs.tsukuba.ac.jp

***Abstract*—This paper proposes multiscale directional transforms (MDTs) based on cosine-sine modulated filter banks (CSMFBs). Sparse image representation by directional transforms is necessary for image analysis and processing tasks and has been extensively studied. Conventionally, cosine-sine modulated filter banks (CSMFBs) have been proposed as one of separable directional transforms (SepDTs). Their computational cost is much lower than non-SepDTs, and they can work better than other SepDTs, e.g., dual-tree complex wavelet transforms (DTCWTs) in image processing applications. One drawback of CSMFBs is a lack of multiscale directional selectivity, i.e., it cannot provide multiple scale directional atoms as in the DTCWT frame, and thus flexible image representation cannot be achieved. In this work, we show a design method of multiscale CSMFBs by extending modulated lapped transforms, which are a subclass of CSMFBs. We confirm its effectiveness in nonlinear approximation and image denoising as a practical application.**

I. Introduction

Directional transforms (DTs) such as *dual-tree complex wavelet transforms* (DTCWTs) [**?**], [**?**], *Contourlet* [**?**], *Curvelet* [**?**], and so on, have been widely studied for their efficiency of sparse image representation. Among DTs, DTCWTs have gathered much attention due to their low computational complexity [**?**], [**?**]. While two dimensional non-separable (non-Sep) DTs usually require high computational complexity, DTCWTs, which is a subclass of 2D SepDTs, can save computational complexity by a parallel 2D separable implementation of two filter banks (FBs), i.e., filtering along vertical and horizontal directions. Thanks to DS, it can be successfully applied to various kinds of practical image processing, such as image denoising, image analysis, and image compression [**?**].

As well as the DTCWT, cosine-sine modulated filter banks (CSMFBs) have been shown as another SepDTs [**?**], [**?**], [**?**]. One problem of DTCWTs is the difficulty in designing M-channel DTCWT with good filter performances, e.g., stopband attenuation or coding gain, since the fractional delay requirement between two FBs has to be approximated. On the other hand, CSMFBs require NO fractional delay (just the modulation of a prototype filter), and thus it is easier to design M-channel CSMFBs with better performance than M-channel DTCWTs.

One problem on the conventional CSMFBs is a lack of multiscale directional selectivity, i.e., it cannot provide multiscale directional atoms in their frame. DTCWTs, which is known as the class of multiscale directional transforms (MDTs), can sparsely express an input image with multiscale directional atoms by cascading the first and the second FBs to each lowpass subbands. On the other hand, as it will be explained, if CSMFBs are applied to images in the same way of the DTCWT, multiscale directional image representation cannot be achieved.

This paper attempts to design MDTs based on CSMFBs. For that, modulated lapped transforms (MLTs), which is a subclass of the CSMFB, are used. Although MDTs cannot be realized by using MLTs directly, this paper clarifies that a shifted MLT can realize the MDTs. The resulting transform is termed as "multiscale directional MLT (MDMLT)". Experimental results of nonlinear approximation and image denoising show that the MDMLT can reduce the ringing artifact compared with the conventional CSMFBs.

The rest of this paper is organized as follows. Sec. II briefly reviews about the CSMFB. The MDMLTs are presented in Sec. III. Sec. IV evaluates the MDMLT in nonlinear approximation and image denoising. Finally, this paper is concluded in Sec. V.

Notations: $H(z)$ is defined as $H(z) := \sum_n h(n)z^{-n}$. $H(\omega) := \sum_n h(n)e^{-j\omega n}$, $H(\boldsymbol{\omega}) := H(\omega_1, \omega_2) = \sum_{n_1,n_2} h(n_1, n_2)e^{-j(\omega_1 n_1 + \omega_2 n_2)}$. $H_{k_1,k_2}(\boldsymbol{\omega}) := H_{k_1}(\omega_1)H_{k_2}(\omega_2)$. $W_N = e^{j\frac{2\pi}{N}}$. The $M \times L$ FB means the M-channel filter bank with the filter length of L. $\mathbf{I}_N$, $\mathbf{J}_N \in \mathbb{R}^{N\times N}$ are the identity and the reversal identity, respectively. $\mathrm{diag}(\mathbf{A}_0, \ldots, \mathbf{A}_{N-1})$ is a diagonal matrix. $\otimes$ denotes the Kronecker product.

II. Preliminaries

A CSMFB is constructed two maximally decimated perfect reconstruction FBs, as illustrated in Fig. 1. The filter coef-

This work was supported in part by JSPS Grants-in-Aid (16K18100 and 17K14683).

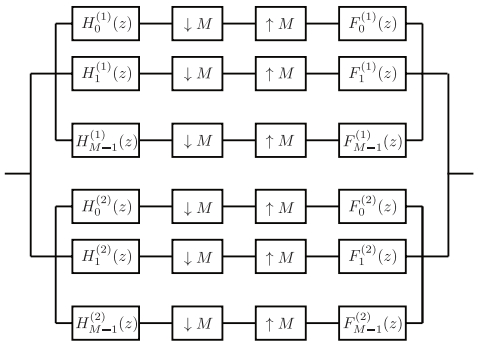

Fig. 1. M-channel CSMFBs

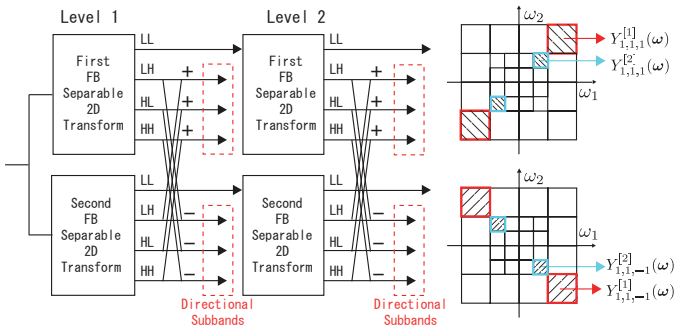

Fig. 2. The configuration to obtain directional subband signals in the 2D frequency plane (the number of channel: $M = 2$).

ficients of $\{H_k^{(1)}(z), H_k^{(2)}(z)\}$ of CSMFBs are expressed as follows [**?**]:

$$h_k^{(1)}(n) := 2p(n)c_{k,n} = 2p(n)\cos(\theta(k,n)) \quad (1)$$

$$h_k^{(2)}(n) := 2p(n)s_{k,n} = 2p(n)\sin(\theta(k,n)) \quad (2)$$

$$\theta(k,n) = \frac{\pi}{M}\left(k+\frac{1}{2}\right)\left(n-\frac{N-1}{2}\right)+\varphi_k \quad (3)$$

where $k = 0,\ldots,M-1$, $N = 2mM$ is the filter length, $n = 0,\ldots,N-1$, $\varphi_k = (-1)^k\frac{\pi}{4}$ and $p(n)$ is the prototype filter. Equivalently, these filters can be represented in the z-domain as follows:

$$\begin{cases} H_k^{(1)}(z) := c_k U_k(z) + \overline{c_k} V_k(z) \\ H_k^{(2)}(z) := -j(c_k U_k(z) - \overline{c_k} V_k(z)) \end{cases}$$
$$U_k(z) = P\left(zW_{2M}^{k+\frac{1}{2}}\right), \quad V_k(z) = P\left(zW_{2M}^{-(k+\frac{1}{2})}\right)$$
$$F_k^{(1)}(z) = z^{N-1}H_k^{(1)}(z^{-1}), \quad F_k^{(2)}(z) = z^{N-1}H_k^{(2)}(z^{-1}). \quad (4)$$

where $P(z)$ is the z-transform of the prototype filter and $c_k = e^{j\varphi_k}W_{2M}^{(k+\frac{1}{2})\frac{N-1}{2}}$. The frequency spectra $U_k(\omega)$ and $V_k(\omega)$, which are modulations of the prototype filter, are lying only in the positive and the negative domain, respectively. According to the above setting, if the first system satisfies the perfect reconstruction (PR) property, the whole system also satisfies the PR property [**?**].

DTCWTs also consists of two maximally decimated FBs as shown in Fig. 1 [**?**]. However, the pairs of subband filters should satisfy the fractional sample delay condition. Since it is difficult to approximate the fractional delay with FIR filters, the resulting filter performance and efficiency in practical application are worse than CSMFBs.

III. Multiscale Modulated Lapped Transforms

A. Lack of directionality

Before introducing the proposed transform, this section mentions the shortage of the CSMFB, i.e., lack of multiscale directionality. To obtain the directional subband signal with CSMFBs at the first scale $J = 1$, the first and the second FB are separably performed along vertical and horizontal directions. Then, output signals from each FBs are added/subtracted as illustrated in Fig. 2. Finally, directional subband signals with twice number of samples of the input image can be obtained. For example, in the case of the number of channel $M = 2$, in order to obtain the $Y_{1,1,1}^{[1]}(\boldsymbol{\omega})$ and $Y_{1,1,-1}^{[1]}(\boldsymbol{\omega})$, the following operation is performed to input image;

$$Y_{k_1,k_2,\pm1}^{[1]}(\boldsymbol{\omega}) = \left(H_{k1,k2}^{(1)}(\boldsymbol{\omega}) \pm H_{k1,k2}^{(2)}(\boldsymbol{\omega})\right)X(\boldsymbol{\omega})$$
$$= \begin{cases} (U_{k_1}(\omega_1)U_{k_2}(\omega_2) + V_{k_1}(\omega_1)V_{k_2}(\omega_2))\,X(\boldsymbol{\omega}) \\ (U_{k_1}(\omega_1)V_{k_2}(\omega_2) + V_{k_1}(\omega_1)U_{k_2}(\omega_2))\,X(\boldsymbol{\omega}) \end{cases}$$

In the case of the DTCWT, directionality can be achieved at any scale as described in the configuration in Fig. 2. However, this procedure does not work in the CSMFB case at higher decomposition levels $J > 1$. For example, in the second scale $J = 2$, from the definition of the subband filters in the CSMFB, the following equation can be verified.

$$H_{k_1,k_2}^{(1)}(2\boldsymbol{\omega})H_{0,0}^{(1)}(\boldsymbol{\omega})X(\boldsymbol{\omega}) \pm H_{k_1,k_2}^{(2)}(2\boldsymbol{\omega})H_{0,0}^{(2)}(\boldsymbol{\omega})X(\boldsymbol{\omega})$$
$$= Y_{k_1,k_2,\pm1}^{[2]}(\boldsymbol{\omega}) + \Delta \neq Y_{k_1,k_2,\pm1}^{[2]}(\boldsymbol{\omega}), \quad (5)$$

where Δ includes the frequency components except the (k_1,k_2) subband. Fig. 3(b) shows (the half of) the second level directional subband coefficients of the test image *Zoneplate* (Fig. 3(a)). The CSMFB cannot distinguish $\pm45^\circ$ directions at the second level. Therefore, CSMFBs cannot be extended to multiscale decomposition straightforwardly.

B. Subband Filters of MDMLT

To design a MDT based on the CSMFB, we use modulated lapped transforms the prototype filter $p(n)$ and the phase term $\hat{\theta}(k,n)$ of which are defined as follows:

$$\hat{h}_k^{(1)}(n) := p(n)\hat{c}_{k,n} = p(n)\cos(\hat{\theta}(k,n))$$
$$\hat{h}_k^{(2)}(n) := p(n)\hat{s}_{k,n} = p(n)\sin(\hat{\theta}(k,n))$$
$$p(n) = -\sqrt{\frac{\pi}{M}}\sin\left(\frac{\pi}{2M}\left(n+\frac{1}{2}\right)\right)$$
$$\hat{\theta}(k,n) = \frac{\pi}{M}\left(k+\frac{1}{2}\right)\left(n+\frac{M+1}{2}\right) \quad (6)$$

For the number of channel M, the filter length of the MLT is $2M$. Since it can be verified that $c_{k,n} = (-1)^{\sigma(k)}\hat{c}_{k,N-1-n}$ ($\sigma(k) = 0$ or 1, $c_{k,n}$ is in (1)), the MLT can be considered

as a subclass of the CSMFB. Based on the prototype filter, we derive the following relationship between the first and the second lowpass filters:

Theorem 1:

$$\begin{aligned}\hat{h}_0^{(2)}\left(n-\frac{M}{2}\right) &= p\left(n-\frac{M}{2}\right)\hat{s}_{0,n-\frac{M}{2}} \\ &= -p(n)\hat{c}_{0,n} = -\hat{h}_0^{(1)}(n) \end{aligned} \quad (7)$$

Proof: From the following equations:

$$\hat{s}_{0,n-\frac{M}{2}} = \sin\left(\frac{\pi}{M}\frac{1}{2}\left(n+\frac{1}{2}\right)\right) = -p(n)$$

$$p\left(n-\frac{M}{2}\right) = -\sin\left(\frac{\pi}{2M}\left(n+\frac{M+1}{2}-M\right)\right) = \hat{c}_{0,n},$$

we can derive the theorem. ■

This indicates that the 2D frequency response of the 2D separable filter of the first and the second FBs are identical:

$$\begin{aligned}\hat{H}_{0,0}^{(1)}(\boldsymbol{\omega}) &= \hat{H}_0^{(1)}(\omega_1)\hat{H}_0^{(1)}(\omega_2) \\ &= \hat{H}_0^{(2)}(\omega_1)\hat{H}_0^{(2)}(\omega_2) = \hat{H}_{0,0}^{(2)}(\boldsymbol{\omega}). \end{aligned} \quad (8)$$

With this in mind, we define the (analysis) subband filters of MDMLT as:

$$\begin{aligned}\hat{h}_k^{(1)}(n) &= p(n)\hat{c}_{k,n} \\ \hat{h}_k^{(2)}(n) &= \begin{cases} p\left(n-\frac{M}{2}\right)\hat{s}_{0,n-\frac{M}{2}} & (k=0,\ J<J_{\max}) \\ p(n)\hat{s}_{0,n} & (k=0,\ J=J_{\max}) \\ p(n)\hat{s}_{k,n} & (k\neq 0) \end{cases} \end{aligned} \quad (9)$$

According to the above setting, we can realize the MDMLT, which can be verified by analyzing the 2D frequency responses at the higher scale. For example, at the second scale $J=2$, we can derive as

$$\begin{aligned}&\hat{H}_{k_1,k_2}^{(1)}(2\boldsymbol{\omega})\hat{H}_{0,0}^{(1)}(\boldsymbol{\omega})X(\boldsymbol{\omega}) \pm \hat{H}_{k_1,k_2}^{(2)}(2\boldsymbol{\omega})\hat{H}_{0,0}^{(2)}(\boldsymbol{\omega})X(\boldsymbol{\omega}) \\ &= (\hat{H}_{k_1,k_2}^{(1)}(2\boldsymbol{\omega}) \pm \hat{H}_{k_1,k_2}^{(2)}(2\boldsymbol{\omega}))\hat{H}_{0,0}^{(1)}(\boldsymbol{\omega})X(\boldsymbol{\omega}) \\ &= \begin{cases} (U_{k_1}(2\omega_1)U_{k_2}(2\omega_2) + V_{k_1}(2\omega_1)V_{k_2}(2\omega_2))\,\hat{H}_{0,0}^{(1)}(\boldsymbol{\omega})X(\boldsymbol{\omega}) \\ (U_{k_1}(2\omega_1)V_{k_2}(2\omega_2) + V_{k_1}(2\omega_1)U_{k_2}(2\omega_2))\,\hat{H}_{0,0}^{(1)}(\boldsymbol{\omega})X(\boldsymbol{\omega}) \end{cases} \\ &= Y_{k_1,k_2,\pm 1}^{[2]}(\boldsymbol{\omega}). \end{aligned} \quad (10)$$

It indicates that the proposed MDMLT, the redundancy ratio is 2, has multiscale directionality. Fig. 3(c) shows (the half of) the second level directional subband coefficients of the test image *Zoneplate* (Fig. 3(a)). In this case, the MDMLT can distinguish $\pm 45^\circ$ directions at the second level.

C. Inverse Transform of MDMLT

Now, we consider the inverse transform of the proposed MDMLT. While the first FB $\{\hat{h}_k^{(1)}(n)\}$ is invertible by setting synthesis filter $\{\hat{f}_k^{(1)}(n)\}$ as in (4), the second FB $\{\hat{h}_k^{(2)}(n)\}$ is not since its lowpass filter is shifted by $\frac{M}{2}$ samples.

To derive the inverse transform, we first describe the forward transform with $J_{\max}$ level decomposition by using the expression from the viewpoint of a matrix multiplication as:

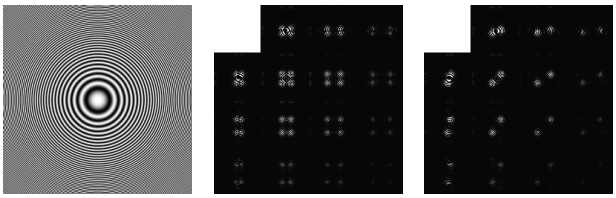

(a) (b) (c)

Fig. 3. (a) *Zone plate*, (b) (half of) second level transformed coeff. of the CSMFB, (c) (half of) second level transformed coeff. of the MDMLT.

$$\mathbf{H} = \mathbf{W}\mathbf{T}^{[J_{\max}]}\left(\prod_{J=2}^{J_{\max}-1}\mathbf{T}^{[J]}\right)\mathbf{T}^{[1]},$$

$$\mathbf{W} = \frac{1}{\sqrt{2}}\begin{bmatrix}\mathbf{I}_{N^2} & \mathbf{I}_{N^2} \\ \mathbf{I}_{N^2} & -\mathbf{I}_{N^2}\end{bmatrix},\ \mathbf{T}^{[1]} = \begin{bmatrix}\mathbf{T}_1^{[1]} \\ \mathbf{T}_2^{[1]}\end{bmatrix} = \begin{bmatrix}\mathbf{C}^{[1]}\otimes\mathbf{C}^{[1]} \\ \mathbf{S}^{[1]}\otimes\mathbf{S}^{[1]}\end{bmatrix}$$

$$\mathbf{T}^{[J]} = \mathrm{diag}(\mathbf{T}_1^{[J]}, \mathbf{T}_2^{[J]}),\ \mathbf{T}_1^{[J]} = \mathrm{diag}(\mathbf{C}^{[J]}\otimes\mathbf{C}^{[J]}, \mathbf{I}_{N^2-(\frac{N}{M^J})^2})$$

$$\mathbf{T}_2^{[J]} = \mathrm{diag}(\mathbf{S}^{[J]}\otimes\mathbf{S}^{[J]}, \mathbf{I}_{N^2-(\frac{N}{M^J})^2}), \quad (11)$$

where the matrices $\mathbf{C}^{[J]},\ \mathbf{S}^{[J]} \in \mathbb{R}^{N/M^J\times N/M^J}$ denote 2D separable transform of $\{\hat{h}_k^{(1)}(n)\}$, $\{\hat{h}_k^{(2)}(n)\}$ with downsampling at J-th scale. Then, the inverse transform $\mathbf{F}$ can be given by the Moore-Penrose pseudo-inverse matrix as:

$$\mathbf{F} = \left(\mathbf{H}^\top\mathbf{H}\right)^{-1}\mathbf{H}^\top. \quad (12)$$

Since the MLT is paraunitary FB, i.e., $(\mathbf{C}^{[J]}\otimes\mathbf{C}^{[J]})^\top(\mathbf{C}^{[J]}\otimes\mathbf{C}^{[J]}) = \mathbf{I}$, $(\mathbf{S}^{[J]}\otimes\mathbf{S}^{[J]})^\top(\mathbf{S}^{[J]}\otimes\mathbf{S}^{[J]}) = \mathbf{I}$,

$$\begin{aligned}\mathbf{F} &= \left(\mathbf{I} + \left(\prod_{J=1}^{J_{\max}-1}\mathbf{T}_2^{[J]}\right)^\top\left(\prod_{J=0}^{J_{\max}-1}\mathbf{T}_2^{[J]}\right)\right)^{-1}\mathbf{H}^\top \\ &= \mathbf{V}\left(\mathbf{I}+\mathbf{D}\right)^{-1}\mathbf{V}^\top\mathbf{H}^\top, \end{aligned} \quad (13)$$

where the unitary matrix $\mathbf{V}$ and the diagonal matrix $\mathbf{D}$ are obtained by the eigenvalue decomposition as: $\left(\prod_{J=0}^{J_{\max}-1}\mathbf{T}_2^{[J]}\right)^\top\left(\prod_{J=0}^{J_{\max}-1}\mathbf{T}_2^{[J]}\right) = \mathbf{V}\mathbf{D}\mathbf{V}^\top$.

1) Two-level Decomposition Case: As shown in (13), the MDMLT requires the eigenvalue decomposition of the huge matrix $\left(\prod_{J=0}^{J_{\max}-1}\mathbf{T}_2^{[J]}\right)^\top\left(\prod_{J=0}^{J_{\max}-1}\mathbf{T}_2^{[J]}\right)$ to find the matrices $\mathbf{V}$ and $\mathbf{D}$, which consumes significant computational cost. For this problem, if we restrict that the number of the decomposition level for MDMLT is 2, more computationally-efficient MDMLT can be designed. The 2-level MDMLT is expressed as:

$$\begin{aligned}\mathbf{H} &= \mathbf{W}\mathbf{T}^{[2]}\mathbf{T}^{[1]} \\ \mathbf{F} &= \left(\mathbf{I} + (\mathbf{S}^{[1]}\otimes\mathbf{S}^{[1]})^\top(\mathbf{S}^{[1]}\otimes\mathbf{S}^{[1]})\right)^{-1}\mathbf{H}^\top \end{aligned} \quad (14)$$

From the eigenvalue decomposition of $\mathbf{S}^{[1]} = \mathbf{U}^{[1]}\mathbf{D}^{[1]}(\mathbf{V}^{[1]})^\top$, we can derive

$$\begin{aligned}\mathbf{F} &= \left(\mathbf{I} + (\mathbf{S}^{[1]}\otimes\mathbf{S}^{[1]})^\top(\mathbf{S}^{[1]}\otimes\mathbf{S}^{[1]})\right)^{-1}\mathbf{H}^\top \\ &= (\mathbf{V}^{[1]}\otimes\mathbf{V}^{[1]})(\mathbf{I}+\mathbf{D}^{[1]})^{-1}(\mathbf{V}^{[1]}\otimes\mathbf{V}^{[1]})^\top\mathbf{H}^\top. \end{aligned} \quad (15)$$

(a) *Lena* (b) *Barbara* (c) *Pepper*

Fig. 4. Original images

TABLE I
THE NUMERICAL RESULTS OF NLA

Zoneplate (256×256)				
Num. of coeff.	2000	3000	4000	5000
8×22 DTCWT	12.57	14.87	16.64	17.83
8×16 CSMFB	14.91	18.93	21.61	24.22
64×128 CSMFB	11.11	11.93	12.71	13.47
8×16 MDMLT (Prop.)	**18.06**	**20.51**	**22.99**	**25.02**
Barbara (512×512)				
Num. of coeff.	5000	10000	15000	20000
8×22 DTCWT	23.58	26.96	28.84	30.21
8×16 CSMFB	24.18	28.53	30.87	32.57
64×128 CSMFB	25.83	27.93	29.38	30.55
8×16 MDMLT (Prop.)	**27.85**	**28.92**	**30.87**	**32.36**

This indicates that, except the element-wise multiplication $(\mathbf{I} + \mathbf{D}^{[1]})^{-1}$, each procedure is implemented as separable transform, and thus the computational complexity can be significantly reduced.

IV. Experimental Results

A. Nonlinear Approximation

This section evaluates the efficiency of the MDMLT by NLA [**?**]. NLA is often used for the evaluation of sparse representation by reconstructing images from the K-largest (magnitude) transformed coefficients $\mathbf{y} = \mathbf{F}\mathbf{x} \xrightarrow[\text{coefficients}]{K-\text{largest}} \widetilde{\mathbf{y}} = \mathbf{F}\widetilde{\mathbf{x}}$. Here we examined the 2-level DTCWTs with the FB size of 8×22, the 1-level CSMFB with the size of 8×16, and the 2-level MDMLT with the size of 8×16. We also compare the 1-level 64×128 CSMFB of which 2D lowpass subband is the same as that of the 2-level 8×16 MDMLT. All the redundancy ratios are 2. *Zoneplate* (256×256 pixels) and *Barbara* (512×512 pixels), which have rich directional textures, are used as test images (512×512 pixels).

Table II shows the reconstruction error (PSNR [dB]) from the number of coefficients retained. It shows the reconstructed images by the proposed method have consistently higher PSNRs compared to those by the conventional ones.

B. Image Denoising

In this section, the performances of the 2-level 8×22 DTCWT, the 1-level 64×128 CSMFB, the 2-level 8×16 MDMLT in image denoising is verified. The test images *Zoneplate*, *Lena*, *Barbara*, and *Pepper*, are added the Gaussian noise with variance σ^2 $(\sigma = 20)$. Directional transforms first decompose the noisy images, then hard-thresholding with 3σ is performed. From Fig. 5, since the CSMFB requires a large support of atoms to decompose the lowpass frequency region finely, the resulting image of the CSMFB is significantly degraded with severe ringing artifacts. On the other hand, the denoising result of the MDMLT provides better visual quality

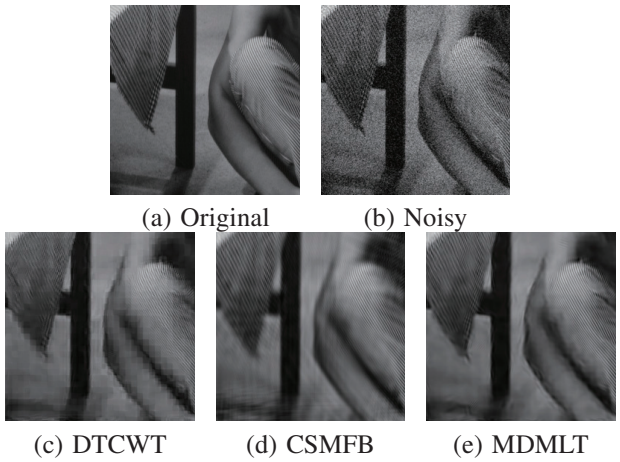

(a) Original (b) Noisy

(c) DTCWT (d) CSMFB (e) MDMLT

Fig. 5. Original, noisy, and denoise images of *Barbara*.

TABLE II
THE NUMERICAL RESULTS OF IMAGE DENOISING (PSNR [DB])

Test image	*Zoneplate*	*Lena*	*Barbara*	*Pepper*
Noisy image	22.12	22.12	22.12	22.12
8×22 DTCWT [**?**]	23.34	28.88	27.10	28.96
64×128 CSMFB [**?**]	23.47	28.55	26.97	28.25
8×16 MDMLT	**27.83**	**29.79**	**28.43**	**29.70**

than the DTCWT due to flexible multiscale directional image representation.

V. Conclusions

In this paper, we proposed the MDMLT as a multiscale directional transform. To construct the MDMLT, we first derived the relationship between the lowpass filter of the first FB and the shifted lowpass filter of the second FB. Then, we designed the MDMLT based on the MLT and the shifted MLT. Finally, in the NLA and image denoising simulations, it was clarified that the proposed MDMLT provides better numerical and visual reconstruction quality compared with the conventional CSMFBs and the DTCWTs.

References

[1] R. G. Baraniuk I. W. Selesnick and N. G. Kingsbury, "The dual-tree complex wavelet transform," *IEEE Signal Process. Mag.*, pp. 123–151, Nov. 2005.

[2] I. Bayram and I.W. Selesnick, "On the dual-tree complex wavelet packet and M-band transforms," *IEEE Trans. Signal Process.*, vol. 56, no. 6, pp. 2298–2310, June 2008.

[3] M. N. Do and M. Vetterli, "The contourlet transform : An efficient directional multiresolution image representation," *IEEE Trans. Image Process.*, vol. 14, no. 12, pp. 2091–2106, 2005.

[4] E. J. Candès and D. L. Donoho, "New tight frames of curvelets and optimal representations of objects with piecewise C^2 singularities," *Comm. Pure Appl. Math*, vol. 56, no. 2, pp. 219–266, Feb. 2004.

[5] S. Kyochi, T. Uto, and M. Ikehara, "Dual-tree complex wavelet transform arising from cosine-sine modulated filter banks," in *Proc. IEEE Int. Symp. Circuits Syst.*, May 2009, pp. 2189–2192.

[6] S. Kyochi and M. Ikehara, "A class of near shift-invariant and orientation-selective transform based on delay-less oversampled evenstacked cosine-modulated filter banks," *IEICE Trans. Fundam. Electron, Commun. Comput,*, vol. E93-A, pp. 724–733, Apr. 2010.

[7] L. Liang and H. Liu, "Dual-tree cosine-modulated filter bank with linear-phase individual filters: An alternative shift-invariant and directional-selective transform," *IEEE Trans. Image Process.*, vol. 22, no. 12, pp. 5168–5180, Dec. 2013.

[8] Stphane Mallat, *A Wavelet Tour of Signal Processing, Third Edition: The Sparse Way*, Academic Press, 3rd edition, 2008.